Dynamic radial distribution function from inelastic neutron scattering

R. J. McQueeney
Lujan Center, Los Alamos Neutron Science Center, Los Alamos National Laboratory, Los Alamos, New Mexico 87545
(Received 16 September 1997; revised manuscript received 1 December 1997)

A real-space, local dynamic structure function $g(r,\omega)$ is defined from the dynamic structure function $S(Q,\omega)$, which can be measured using inelastic neutron scattering. At any particular frequency ω, $S(Q,\omega)$ contains Q-dependent intensity oscillations which reflect the spatial distribution and relative displacement directions for the atoms vibrating at that frequency. Information about local and dynamic atomic correlations is obtained from the Fourier transform of these oscillations $g(r,\omega)$ at the particular frequency. $g(r,\omega)$ can be formulated such that the elastic and frequency-summed limits correspond to the average and instantaneous radial distribution function, respectively, and is thus called the dynamic radial distribution function. As an example, the dynamic radial distribution function is calculated for fcc nickel in a model which considers only the harmonic atomic displacements due to phonons. The results of these calculations demonstrate that the magnitude of the atomic correlations can be quantified and $g(r,\omega)$ is a well-defined correlation function. This leads to a simple prescription for investigating local lattice dynamics. [S0163-1829(98)00817-0]

I. INTRODUCTION

Recently, much attention has been focused on problems related to the local atomic structure and dynamics of many different materials. For amorphous materials, the short wavelength lattice vibrations are necessarily local in nature and contain additional information about the atomic structure. In materials such as high-temperature superconductors and colossal magnetoresistors, electron-lattice coupling induces local atomic displacements which have been observed by local structural probes such as neutron and x-ray pair-distribution function (PDF) analysis, extended x-ray absorption fine structure (EXAFS), NQR, and NMR.[1–3] In such cases, it is also important to determine the dynamic nature of the local atomic correlations which are not given by the above measurements. The dynamic response of atoms gives an indication of the underlying charge dynamics at the least, and may imply a more profound interaction between electrons and the lattice, such as polaron formation. A major obstacle in resolving this problem arises precisely from this local nature. The full characterization of local phenomena exists in a gap amongst various experimental techniques. While many truly local probes do exist, such as diffraction PDF analysis, NMR, NQR, and EXAFS, these probes have characteristic time scales which are either too slow or too fast to capture the local atomic dynamics. However, inelastic neutron scattering is exceptional, and has the capability to resolve both local and dynamic features. With the advent of high resolution, high intensity pulsed-neutron chopper spectrometers at spallation sources (such as PHAROS at LANSCE and MARI at the ISIS facility), it has been possible to measure the full dynamic scattering function $S(Q,\omega)$ up to very large momentum transfers ($Q\sim 20-30$ Å^{-1} or more). In particular, the Q dependence of the intensity at constant frequency gives information about the spatial distribution and relative displacements of atoms vibrating at that frequency. In principle, one should be able to ascertain the local dynamics contained in the Q dependence by using Fourier methods to extract $g(r,\omega)$, a real-space dynamic structure function.

The concept of a real-space dynamic structure function was introduced in the seminal theoretical papers by Carpenter and Pelizzari.[4,5] Local dynamic pair-correlation functions (DPCF) have been obtained experimentally by Arai *et al.* and Hannon *et al.*, for amorphous Boron,[6] amorphous g-SiO_2,[7–9] and a polycrystalline $YBa_2Cu_3O_7$ superconductor,[9,10] using inelastic neutron scattering. The DPCF obtained for a certain frequency resembles the neutron PDF obtained from Fourier transformation of the diffraction data. The DPCF contains peaks corresponding to the atomic pair positions (or coordination shells) which have coherent density oscillations at that frequency. The DPCF peaks can be positive or negative, which signifies the in-phase or out-of-phase motion of the atomic pair. For amorphous materials, the above authors have demonstrated that the DPCF gives additional structural information beyond that available from diffraction techniques.

In addition, the intensities (and signs) of the DPCF peaks should in principle be used for determining other details of the correlated motion, such as the magnitude. However, as Hannon *et al.* point out,[6,7] the DPCF is not a true correlation function and peaks in the r dependence at a given frequency can contain fictitious, long tails. Whereas, the PDF [or more formally the radial distribution function (RDF)] measures the probability that two atoms are separated by a distance r, the DPCF has no such interpretation. This arises from the precise Fourier transform kernel used to obtain the DPCF from the inelastic neutron data. In the present paper, we examine the properties of $g(r,\omega)$ by Fourier transformation of the dynamic scattering function $S(Q,\omega)$ using a simple variation of the DPCF analysis. By doing so, one restores a probabilistic interpretation of $g(r,\omega)$. This is evidenced by the fact that the average RDF [elastic, $g(r,\omega=0)$] and instantaneous RDF [frequency summed $g(r,\omega)$] are obtained directly from $g(r,\omega)$. The local dynamic function $g(r,\omega)$ is thus called the dynamic radial distribution function.

The interpretation of the instantaneous and average RDF gives more insight into the nature of $g(r,\omega)$. The instantaneous RDF measures the probability of two atoms being

separated by a distance r by averaging ''snap-shots'' of the structure over all time, whereas the average RDF is the probability of two *independently* time-averaged atoms being a certain distance apart.[11] Thus, differences in the instantaneous and average RDFs imply the existence of correlated atomic motions. The ω dependence at constant r can then be used to determine the frequencies of such correlated motion. Finally, comparison of $g(r,\omega)$ to the intensity of the average (uncorrelated) RDF peak $g(r,\omega=0)$ quantifies the strength of the atomic correlations.

In order to test these ideas, a real-space approach for performing theoretical calculations of the dynamic RDF is developed. While some specifics of this approach are only formally correct for periodic systems, the general results are applicable to amorphous or glassy systems. The correlated atomic motions in a model consisting of harmonic phonons in nickel are considered in this paper and $g(r,\omega)$ is calculated for the first few nearest-neighbor pairs in polycrystalline nickel. A comparison of the instantaneous and average RDFs shows that significant ''in-phase'' atomic correlations (17% of the average RDF intensity) are present for the nearest neighbor atomic pair. The calculated results agree with neutron diffraction RDF measurements of Ni and other materials (such as aluminum, not shown here), where it is observed that nearest neighbor peaks are narrower than those originating from well separated atomic pairs.[12,13] The frequency dependence at the nearest neighbor separation is dominated by the low frequency and long wavelength phonons which tend to move the atomic pair together as a unit.

In this simple example, the local dynamic correlation function determines the involved atomic pairs, their relative displacements, frequency range, and strength of a local correlated motion. It is expected that the following prescription, in conjunction with DPCF methods, will lay a groundwork for the consistent experimental evaluation of local and dynamic atomic correlations in more complicated systems.

II. THEORY

When an inelastic neutron scattering measurement is made on an amorphous or polycrystalline material, the intensity is proportional to $S(Q,\omega)$, the (orientationally averaged) dynamic scattering function. $\hbar Q$ and $\hbar\omega$ are defined as the momentum and energy transferred to the sample. In order to extract the local atomic structure and dynamics (without resorting to modeling), the dynamical scattering function can be Fourier transformed over the spatial coordinates, giving a real-space dynamic function $g(r,\omega)$.

The procedure for obtaining $g(r,\omega)$ begins by separating the data into several Q-dependent cuts each covering a different range of frequencies. The chosen frequency range for each cut depends on the finite energy transfer binning in the experiment, but can be as small as the energy resolution of the spectrometer, or as large as one wishes. Thus, in this case, ω is an average quantity over some specified frequency range. We can write a general spatial Fourier transform for each Q cut as

$$g(r,\omega)=\frac{2r}{\pi}\int_0^\infty QdQ\ \sin(Qr)f(Q)[S(Q,\omega)-B(Q,\omega)], \tag{1}$$

where $B(Q,\omega)$ is a slowly varying intensity component which arises from incoherent, multiple, multiphonon scattering and the instrumental background. This must be modeled (or fitted) and subtracted for each ω in order to perform the Fourier transformation without termination errors. Thus, $S(Q,\omega)$-$B(Q,\omega)$ is intended to represent the coherent inelastic scattering. $f(Q)$ is a weighting function whose choice determines the functional form of the radial part of $g(r,\omega)$, as will be shown later.

Previous authors[6–9] have included a Q-dependent weighting function $f(Q)=1/Q^2$. The resulting function, referred to previously, is called the dynamic pair-correlation function DPCF by the authors. The use of this weighting function has merit and the reason for this particular choice is discussed in the Appendix.

In the present paper, a weighing factor $f(Q)=1$ is chosen. This transformation is entirely analogous to the pair-distribution function (PDF) analysis of diffraction data.[11] [The pair distribution function $\rho(r)$ and the radial distribution function (RDF) $g(r)$ are simply related by the equation $g(r)=4\pi r^2\rho(r)$.] In fact, by making this choice the elastic component $g(r,\omega=0)$ and the frequency summed $g(r,\omega)$ (the frequency range spanning the entire data set) are precisely the average and instantaneous RDFs. These are extremely important limits since the interpretation of the average and instantaneous RDFs is well defined. This is demonstrated by introducing the general pair correlation function $G(r,t)\propto\langle g_i(t')g_j(t-t')\rangle_{t'}$, which is averaged over all possible initial times t' for two atoms labeled i and j separated by a distance r. The dynamic radial distribution function is just the time Fourier transform of $G(r,t)$:

$$g(r,\omega)\propto\int dte^{i\omega t}\langle g_i(t')g_j(t-t')\rangle_{t'}. \tag{2}$$

The interpretation of the average RDF as the probability of separation by r when each atomic position is averaged *independently* over time follows simply from Eq. (2)

$$g(r,\omega=0)\propto\int dt\langle g_i(t')g_j(t-t')\rangle_{t'}=\langle g_i(t)\rangle_t\langle g_j(t)\rangle_t. \tag{3}$$

Being a single-atom average over the atomic motions, the average RDF contains no atomic correlation. The instantaneous RDF, given by the sum over all frequencies, is seen as the average over all time of successive ''snap-shots'' of the atomic structure:

$$\begin{aligned} g(r)&=\int d\omega g(r,\omega)\propto\int d\omega\int dte^{i\omega t}\langle g_i(t')g_j(t-t')\rangle_{t'}\\ &=\int dt\langle g_i(t')g_j(t-t')\rangle_{t'}\delta(t)=\langle g_i(t)g_j(t)\rangle_t. \end{aligned} \tag{4}$$

Differences between the instantaneous and average RDF are a signature of local and dynamic atomic correlation.

Instantaneous RDFs are obtained from x-ray and pulsed-neutron diffraction since these techniques sum over all energy transfers. In order to obtain the average RDF, an inelastic experiment is a necessity. Thus, with an inelastic neutron scattering measurement of $S(Q,\omega)$ using a pulsed-neutron chopper spectrometer, one is able to obtain both the instan-

taneous and average RDFs from the same data set. Despite the fact that the Q resolution is significantly better in a diffraction experiment, the RDFs obtained from inelastic measurements compare quite favorably to diffraction results.[14] Of course, the strength of the inelastic measurement lies in the possibility to determine which frequency range contributes most significantly to the differences in the instantaneous and average RDF. Analysis of the details of $g(r,\omega)$ can determine the nature of the correlation, such as in-phase or out-of phase displacements. The end result is the measurement of the frequency and relative displacements of the local correlated motion between a given pair of atoms.

In order to examine these ideas, we calculate $g(r,\omega)$ for a simple crystalline system consisting of harmonic atomic displacements due to phonons. We proceed with the calculation from the perspective of the van Hove scattering function. The phonon expansion of $S(\mathbf{Q},\omega)$ is given by the sum of elastic, one-phonon, and multiphonon terms[15]

$$S(\mathbf{Q},\omega)=S_0(\mathbf{Q},\omega)+S_1(\mathbf{Q},\omega)+S_m(\mathbf{Q},\omega), \tag{5}$$

The elastic and one-phonon terms are given by the equations to be summed over all pairs of atoms in the system

$$S_0(\mathbf{Q},\omega)=\frac{1}{\langle b^2\rangle}\,\delta(\omega)\sum_{ij}\, b_i b_j e^{-W_i-W_j} e^{i\mathbf{Q}\cdot\mathbf{R}_{ij}}, \tag{6a}$$

$$\begin{aligned} S_1(\mathbf{Q},\omega)=&\frac{1}{N\langle b^2\rangle}\,\frac{\hbar^2Q^2}{2\omega}\,[n(\omega)+1]\\ &\times\sum_{ij}\,\frac{b_i b_j e^{-W_i-W_j}}{\sqrt{M_iM_j}}\,e^{i\mathbf{Q}\cdot\mathbf{R}_{ij}}\\ &\times\sum_{\mathbf{q}\nu}\,[\hat{Q}\cdot\hat{\varepsilon}_i(\mathbf{q}\nu)]^*[\hat{Q}\cdot\hat{\varepsilon}_j(\mathbf{q}\nu)]e^{i\mathbf{q}\cdot\mathbf{R}_{ij}}\\ &\times\delta(\omega-\omega_\nu(\mathbf{q})). \end{aligned} \tag{6b}$$

For these formulas, $i(j)$ labels the atoms of mass $M_{i(j)}$ and (coherent) scattering length $b_{i(j)}$ within the crystal, $\mathbf{R}_{ij}$ is the vector joining the atoms, $n(\omega)$ is the Bose filling factor, $\mathbf{q}$ is the phonon wave vector in the first Brillouin zone, $\omega_\nu(\mathbf{q})$ is the phonon dispersion relation with ν labeling the different phonon branches, and $\boldsymbol{\varepsilon}_i(\mathbf{q}\nu)$ is the atomic polarization vector of the ith atom for the particular phonon mode. The phonon polarizations are defined without the plane-wave phase factor [which is explicit in formula (6b)]. The function $\exp(-W_i)$ is the Debye-Waller factor whose argument $W_i=Q^2\langle u_i^2\rangle/2$, is proportional to the mean-squared atomic displacement of the ith atom. $S_m(\mathbf{Q},\omega)$ is the multiphonon intensity, which is a complicated sum over several phonon events.

For phonons in a crystal, it is common to use the periodicity of the crystal to reduce the sum over atoms to a delta function conserving the crystal momentum for elastic and inelastic scattering. However, in order to relate to an experiment performed on a polycrystalline sample, the above formulas must be orientationally averaged over all directions of $\mathbf{Q}$. If one performs the sum over atoms first, the orientational average is very cumbersome, requiring one to bootstrap through the different Brillouin zones intersected by a sphere of radius Q and calculate the argument of Eq. (6b). Since we are only interested in local real-space information, the sum over atoms is retained and will be evaluated neighbor-by-neighbor over the first few coordination shells. Following Carpenter,[16] the orientational averages of Eqs. (6a) and (6b) are then

$$S_0(Q,\omega)=\frac{1}{\langle b^2\rangle}\,\delta(\omega)\sum_{ij}\, b_i b_j e^{-W_i-W_j} j_0(QR_{ij}), \tag{7a}$$

$$\begin{aligned} S_1(Q,\omega)=&\frac{1}{N\langle b^2\rangle}\,\frac{\hbar^2Q^2}{2\omega}\,(n(\omega)+1)\\ &\times\sum_{ij}\,\sum_{\mathbf{q}\nu}\,\frac{b_i b_j e^{-W_i-W_j}}{\sqrt{M_iM_j}}\,e^{i\mathbf{q}\cdot\mathbf{R}_{ij}}\delta(\omega-\omega_\nu(\mathbf{q}))\\ &\times\Bigg[\frac{1}{3}\,[\hat{\varepsilon}_i(\mathbf{q}\nu)^*\cdot\hat{\varepsilon}_j(\mathbf{q}\nu)][j_0(QR_{ij})+j_2(QR_{ij})]\\ &-[\hat{R}_{ij}\cdot\hat{\varepsilon}_i(\mathbf{q}\nu)]^*[\hat{R}_{ij}\cdot\hat{\varepsilon}_j(\mathbf{q}\nu)]j_2(QR_{ij})\Bigg], \end{aligned} \tag{7b}$$

where $j_0(x)$ and $j_2(x)$ are spherical Bessel functions. It is assumed, for the simple harmonic phonon model, that the polycrystalline average of the multiphonon scattering is slowly varying in Q, and therefore does not contribute to the dynamic atomic structure. This is warranted by estimates of second order (multiphonon) thermal diffuse scattering for a fcc powder.[17] Thus, the following calculations will include only the elastic and one-phonon processes.

The Fourier transform over the spatial coordinates now becomes quite simple. We use Eq. (1) to evaluate the transforms of Eqs. (7a) and (7b) separately. We can easily remove the incoherent scattering by ignoring terms with $i=j$. Since we also do not wish to consider the contribution of multiphonon scattering, for the purposes of calculation, the slowly varying background function $B(Q,\omega)$ is zero. Previous authors[6–9] chose to divide out the Q-dependent terms (Q_2) and/or the ω-dependent terms in the inelastic expression before the transformation. However, we retain them, and the elastic and inelastic parts of the real space dynamic function $g(r,\omega)$ are given below. For the elastic part,

$$g_0(r,\omega)=\frac{1}{\langle b^2\rangle}\,\delta(\omega)\sum_{ij}\, b_i b_j g_0(r-R_{ij}), \tag{8a}$$

where

$$g_0(r-R_{ij})=\frac{2r}{\pi}\int_0^\infty QdQ\,\sin(Qr)j_0(QR_{ij})e^{-W_i-W_j}. \tag{8b}$$

As discussed above, $g_0(r-R)$ is the average RDF of a pair of atoms separated by R. Figure 1(a) shows the typical contribution of a single atomic pair of bondlength R to the average RDF. The average RDF is simply a Gaussian centered at R with peak width given by $\langle u^2\rangle^{1/2}$. The area under the average RDF peak is equal to the number of neighboring atoms in the coordination shell.

The inelastic part can be written as

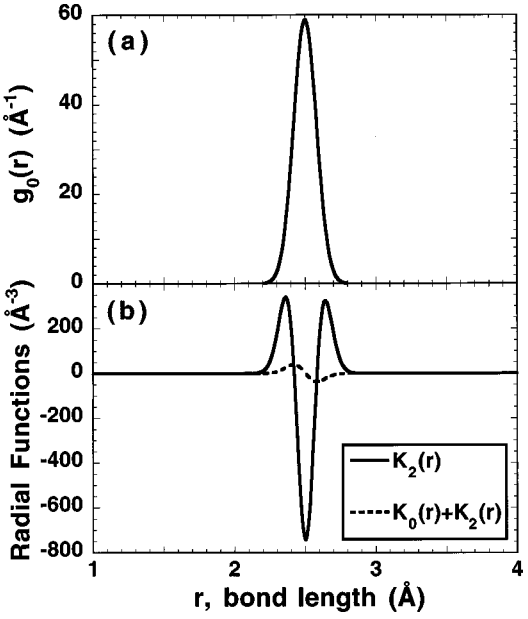

FIG. 1. (a) The radial distribution function peak $g_0(r)$ for elastic scattering from a single coordination shell with equilibrium bondlength $R=2.5$ Å and mean-squared atomic displacement $\langle u^2\rangle = 0.005$ Å^2. (b) The characteristic radial functions related to the one-phonon inelastic scattering $K_2(r)$ and $K_0(r)+K_2(r)$ for the same bondlength and mean-squared displacement as (a). $K_2(r)$ multiplies the longitudinal displacement-displacement correlation function and will narrow or broaden the average RDF when added together. $K_0(r)+K_2(r)$ multiplies the displcement-displacement correlation function and will displace the average RDF peak when added together.

$$g_1(r,\omega)=\frac{1}{\langle b^2\rangle}\sum_{ij} b_i b_j\{F_{ij}(\omega)[K_0(r-R_{ij})+K_2(r-R_{ij})] - F^L_{ij}(\omega)K_2(r-R_{ij})\}, \tag{9a}$$

where the subscript 1 refers to the one-phonon contribution and the functions contained in Eq. (9) are defined as

$$K_n(r-R_{ij})=\frac{2r}{\pi}\int_0^\infty Q^3 dQ\ \sin(Qr)j_n(QR_{ij})e^{-W_i-W_j}, \tag{9b}$$

$$F_{ij}(\omega)=\frac{1}{3N}\frac{\hbar^2}{2\omega\sqrt{M_iM_j}}[n(\omega)+1] \times\sum_{\mathbf{q}\nu}[\hat{\varepsilon}_i(\mathbf{q}\nu)^*\cdot\hat{\varepsilon}_j(\mathbf{q}\nu)]e^{i\mathbf{q}\cdot\mathbf{R}_{ij}}\delta(\omega-\omega_\nu(\mathbf{q})), \tag{9c}$$

$$F^L_{ij}(\omega)=\frac{1}{N}\frac{\hbar^2}{2\omega\sqrt{M_iM_j}}[n(\omega)+1] \times\sum_{\mathbf{q}\nu}[\hat{R}_{ij}\cdot\hat{\varepsilon}_i(\mathbf{q}\nu)]^*[\hat{R}_{ij}\cdot\hat{\varepsilon}_j(\mathbf{q}\nu)]e^{i\mathbf{q}\cdot\mathbf{R}_{ij}} \times\delta(\omega-\omega_\nu(\mathbf{q})). \tag{9d}$$

The inelastic structure function can thus be factored into separate radial and frequency components. The two radial components $K_0(r)+K_2(r)$ and $K_2(r)$ are plotted in Fig. 1(b). It is seen that $K_2(r)$ can be thought of as a ''narrowing'' or ''broadening'' function, depending on the sign of $F^L(\omega)$, when compared to the average RDF. The broadening function, for example, will add intensity to the ends of the average RDF peak in Fig. 1(a) and remove it from the center. In a similar fashion, the sum of the radial functions $K_0(r-R)+K_2(r-R)$ is considered a ''displacement'' function, as it shifts Gaussian weight from one side to the other. An important point to realize is the probability of two atoms being separated by r integrated over all space must equal one whether correlations are included or not. Consequently, the peak areas in both the instantaneous and average RDF must be the same, and are equal to the number of neighboring atoms. The influence of atomic correlation will only redistribute the average RDF intensity. A corollary of this statement is that the integral of the inelastic structure function over all space and frequency must equal zero. When added to the average RDF function, these radial functions tend to change the width or shift the peak while conserving the peak area. A comparison of these radial functions and those of the DPCF of Arai and co-workers is given in the Appendix.

All of the information about the local dynamic atomic correlation is contained within the correlation functions $F(\omega)$ and $F^L(\omega)$. Both functions are evaluated simply by averaging the correlations over the surfaces of constant frequency within the first Brillouin zone of the material. Specifically, $F(\omega)$ is the displacement-displacement correlation function between two atoms, analogous to the spin-spin correlation function measured by magnetic neutron scattering. $F^L(\omega)$ measures the pair displacement correlations along the bond joining the two atoms. The superscript L consequently refers to the longitudinal *pair* correlations. However, it must be stated that this does not imply that the phonons which contribute to this correlation function are necessarily longitudinal. For example, a transverse mode polarized in the (010) direction and propagating in the (100) direction in an fcc crystal has longitudinal pair correlations for the (010) second nearest neighbor atomic pair.

A short comment must be made about the relevance of the above formalism to amorphous or glassy systems. Although, the periodicity of the crystal is not used in the lattice sums during the derivation, the periodicity and symmetry of the crystal is implicit in the Brillouin zone summation of Eqs. (9c) and (9d). The expansion of the lattice dynamics of a glassy system in terms of plane waves (phonons) is not natural, since the lattice momentum is not an eigenstate of a disordered solid. Thus, the above formalism is perhaps not very useful to perform model calculations of disordered systems. However, the general form of Eq. (9a) and the interpretation of the measured correlations holds true for any system in the limit of small vibrational amplitudes and can be utilized for analyzing amorphous systems. Equations (9c) and (9d) simply express a convenient method for calculating the correlation functions in systems with overall long-range periodicity in terms of plane waves. The transformation of the experimental data by Eq. (1) can be used on any system.

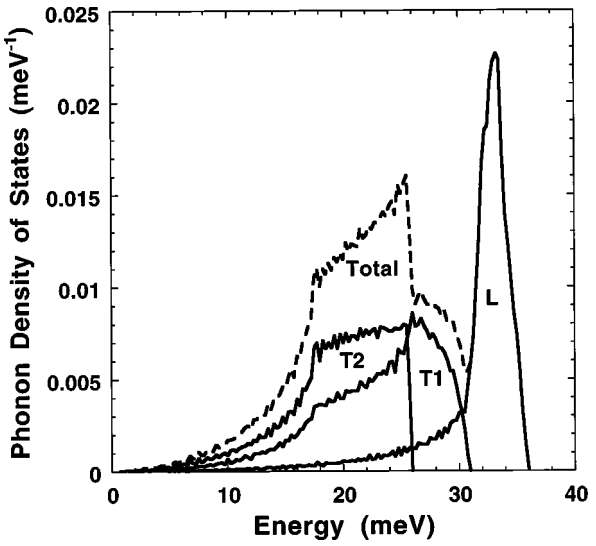

FIG. 2. The normalized phonon density-of-states of Nickel calculated from a five neighbor Born-von Kármán model. The individual longitudinal (L) and transverse ($T1$,$T2$) branches are also shown.

III. MODEL CALCULATIONS ON NICKEL

In the following section, we introduce a simple model to illustrate the ideas of the local, dynamic functions discussed above. The model consists of the harmonic phonon vibrations fcc nickel. The constants for a Born-von Kármán harmonic spring model, including interactions up to the fifth nearest neighbor, were obtained from the literature.[18] These were used to calculate the phonon frequencies and polarization vectors for approximately 67 000 regularly gridded **q** values within an octant of the fcc Brillouin zone. Figure 2 shows the phonon density-of-states $[Z(\omega)]$ obtained from the lattice dynamical calculations by binning the phonon frequencies in 0.25 meV intervals through the Brillouin zone octant after properly weighting the high-symmetry modes.

The radial functions were obtained by calculating the zeroth and second order spherical Bessel functions for 400 Q points from 0 to 60 Å^{-1}. These functions were then Fourier transformed according to Eqs. (8a) and (9b). For a monatomic cubic Bravais lattice, the given formulas can be simplified. The scattering length factor $b_i b_j/\langle b^2\rangle = 1$ and the Debye-Waller factor is obtained from a single mean-squared atomic displacement given by

$$\langle u^2\rangle = \frac{\hbar^2}{2M}\int d\omega\,\frac{Z(\omega)}{\omega}\coth\left(\frac{\hbar\omega}{2kT}\right). \tag{10}$$

Radial functions were calculated for the first four nearest-neighbor shells and the results are identical to Fig. 1, albeit centered at the proper pair distance and broadened by $\langle u^2\rangle$.

Results from the phonon dispersion calculation were used to calculate the correlation functions of Eqs. (9c)–(9d). Considering that nickel is a simple fcc metal with only one atom per unit cell, the phonon polarization vectors defined above are equal at every lattice site (the phase factor is explicitly separated from the phonon eigenvectors). Thus, the arguments of the displacement correlation functions reduce to $\hat{\varepsilon}_i(\mathbf{q}\nu)^*\cdot\hat{\varepsilon}_j(\mathbf{q}\nu)=1$ for $F(\omega)$ and $[\hat{R}_{ij}\cdot\hat{\varepsilon}_i(\mathbf{q}\nu)]^*[\hat{R}_{ij}\cdot\hat{\varepsilon}_j(\mathbf{q}\nu)]=|\hat{R}_{ij}\cdot\hat{\varepsilon}(\mathbf{q}\nu)|^2$ for $F^L(\omega)$. As mentioned previously, the correlation functions are averages over surfaces of constant frequency. In general, the constant frequency surfaces need not be simple, and may be multiply connected as is well known in the case of Fermi surfaces. In the case of $F(\omega)$, the correlation function is proportional to the average phonon phase difference between the pair of atoms for all phonon modes of frequency ω.

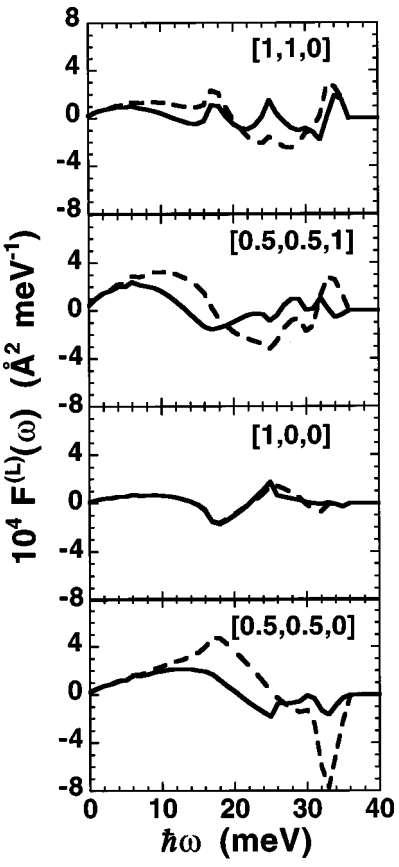

FIG. 3. The frequency-dependent displacement-displacement correlation function $F(\omega)$ (solid line) and longitudinal displacement-displacement correlation function $F^L(\omega)$ (dashed line) for the first four nearest neighbor atomic pairs in nickel at $T=0$ K. The atomic pairs are labeled in the cubic fcc lattice as [0.5,0.5,0], [1,0,0], [0.5,0.5,1], and [1,1,0].

The Brillouin zone sum for $F(\omega)$ can be performed over the reduced zone for any one of the equivalent atomic pairs in a given coordination shell. However, due to the nature of the dot product term remaining in $F^L(\omega)$, the sum over the octant of the Brillouin zone for a single neighbor in a coordination shell is not sufficient to capture all of the contributions to the correlation function. One must either sum over the full zone for a single neighbor, or sum over all neighbors in the reduced zone. We have chosen to use a reduced zone while summing over all pairs in the coordination shell. The results of the Brillouin zone sums were put into 1-meV energy bins and the correlation functions $F(\omega)$ and $F^L(\omega)$ are shown in Fig. 3 for the first four neighbor shells of Ni. Nearest neighbors are labeled by their real space postions in the cubic lattice: [0.5,0.5,0], [1,0,0], [0.5,0.5,1], and [1,1,0].

Some comments are in order about the trends in the correlation functions $F(\omega)$ and $F^L(\omega)$. The first is that the sign

of the correlation function is an indication of the in-phase or out-of-phase motion of an atomic pair. At low frequencies (or long wavelengths) where near by atoms move together, the sign is always positive. Second, the correlation functions tend to oscillate more rapidly as a function of frequency for larger bond distances. This is because the phase difference between atoms will oscillate more rapidly for a larger bond length in the sum over the Brillouin zone. Last, the large peaks in the correlation functions correspond to van Hove singularities in the phonon density of states.

These general trends are easily understood by considering the $F(\omega)$ displacement-displacement correlation function for the nearest neighbor pair. At low frequencies, all three phonon branches move these atoms in the same direction, and $F(\omega)$ is positive. At 24 meV, which is the zone boundary transverse phonon frequency band, the function is negative, indicating that the overall tendency is for nearest neighbor atoms to have opposite displacements. A similar out-of-phase correlation is seen for the longitudinal zone boundary phonon band at 33 meV.

The $F^L(\omega)$ longitudinal displacement-displacement correlation function is dominated by two peaks at 18 and 33 meV, being positive and negative respectively. The 18 meV peak consists mainly of the (111)-type transverse zone boundary phonons. The displacement field of this phonon band tends to move all atoms in every other plane perpendicular to (111) in the same direction. The in-phase motions of some neighboring atoms within each plane point along the bond direction and contribute to the large positive peak at 18 meV. The longitudinal zone boundary phonon band at 33 meV is composed of mainly (100)- and (111)-type phonons. In the longitudinal band, a predominance of atoms in the nearest neighbor shell move in opposite directions along the bond.

The results for the radial and frequency components can be combined according to Eq. (9a) give the full $g_1(r,\omega)$. To determine the influence of the phonon vibrations on the structure [the dependence of $g_1(r,\omega)$ on r] it is most profitable to consider the sum over frequency $g_1(r)$. $g_1(r)$ represents the inelastic contribution of the polycrystalline averaged thermal diffuse scattering to the instantaneous RDF. Since the r- and ω-dependent components in Eq. (9a) are being multiplied, inelastic intensity occurs only where the RDF is nonzero, i.e., only within $\sim\langle u^2\rangle$ of the pair distances [see Fig. 1(b)]. When $g_1(r)$ is added to the average RDF function $g_0(r)$, one obtains the instantaneous RDF $g(r)=g_0(r)+g_1(r)$. All of these radial distribution functions, the average, inelastic, and instantaneous, are shown in Fig. 4. The integral of $g_1(r)$ over r for each peak gives zero as it should, since the total probability is conserved for both instantaneous and average RDFs.

The function $g_1(r)$ represents the local atomic correlation induced by phonons. The main effect of the inelastic structure is to narrow the instantaneous RDF peaks compared to the average RDF. It is apparent that the narrowing is very significant for the first nearest neighbor, and contributes approximately 17% of the instantaneous RDF peak height (the remainder arising from uncorrelated motion). Such a narrowing of the instantaneous RDF peak implies that the atomic motions due to phonons introduce a correlation upon the nearest neighbor pair which tends to move the atoms in-phase. In other words, the atomic pair tends to move together as a unit. Consequently, the probability of measuring the pair at large distances from the equilibrium bond distance at any instant of time is reduced compared to the independent time-averaging of each atom.

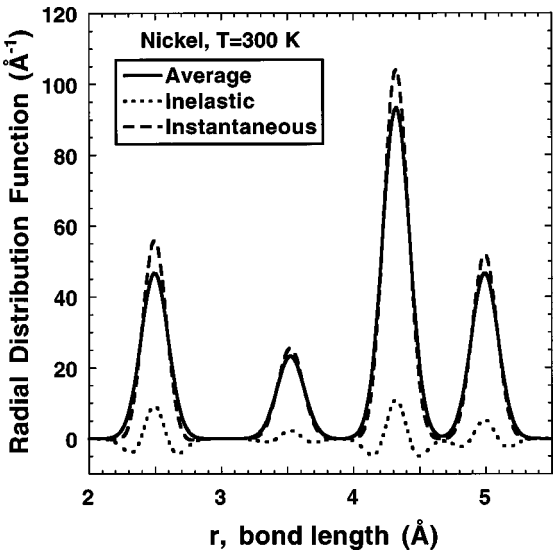

FIG. 4. The average RDF $[g_0(r)]$ and the inelastic RDF $[g_1(r)]$ for the first four nearest neighbors in nickel at $T=300$ K. Also shown is the instantaneous RDF $g(r)$ which is the sum of the average and inelastic RDFs. The figure shows that the instantaneous RDF peak widths are narrower than the average RDF peaks, signifying that there are in-phase correlated motions between the first few nearest neighbors. This is especially true for the first nearest neighbor, where the inelastic RDF contributes 17% of the total instantaneous RDF peak height. The remainder arises from uncorrelated, single-atom motions.

The virtue of the inelastic experiment is that one can determine the frequency ranges which are most responsible for the observed deviations in the instantaneous and average RDFs. This is demonstrated by evaluating the full frequency dependence for $g_1(r=\text{const},\omega)$ precisely at the pair distances, as shown for the first four nearest neighbors in Fig. 5. Due to the different weighting of $K_0(r)+K_2(r)$ and $K_2(r)$ by the $F(\omega)$ and $F^L(\omega)$ correlation functions, respectively, $g_1(r,\omega)$ is a complex function of ω in the vicinity of a pair distance. However, for the case of phonons in nickel, the combination of $K_2(r)F^L(\omega)$ tends to dominate for almost the entire frequency range. This is mainly due to the fact that $K_2(r)$ has a much greater magnitude than $K_0(r)+K_2(r)$ [(as in Fig. 1(b)] while the frequency-dependent correlation functions have equal magnitude (as in Fig. 3). The frequency dependencies in Fig. 5 follow closely the frequency dependence of $F^L(\omega)$. Thus, correlation function which measures the atomic motions along the bond joining the two atoms dominates, and the components of the inelastic structure tend to narrow or broaden the average RDF peaks.

The origin of the dynamic atomic correlations in nickel can be ascertained from Fig. 5. The inelastic intensity at $g(r=\text{first nearest neighbor},\omega)$ has essentially three important contributions. The first is due to the in-phase long wavelength, low frequency modes. The second arises from in-phase atomic correlations of pairs of atoms in planes perpendicular to the transverse mode propagation vectors (18 meV).

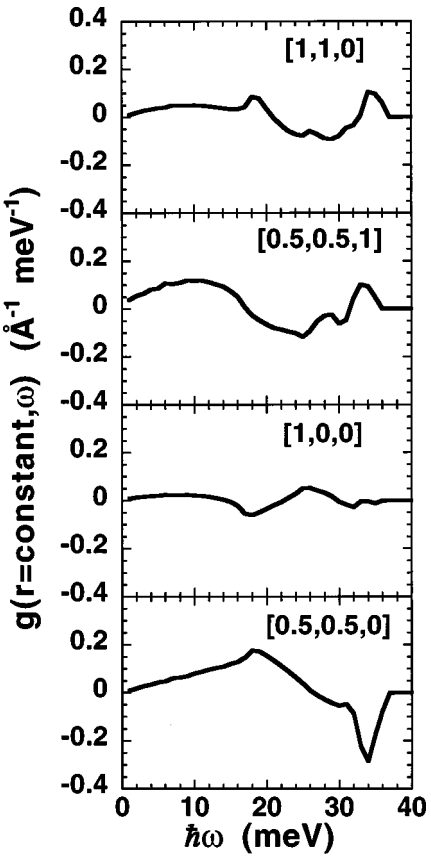

FIG. 5. The dynamic radial distribution function $g(r=\text{const},\omega)$ evaluated at the first four pair distances in nickel at $T=0$ K. The atomic pairs are labeled in the cubic fcc lattice as [0.5,0.5,0], [1,0,0], [0.5,0.5,1], and [1,1,0]. For each neighbor, the frequency dependence is dominated by the longitudinal displacement-displacement correlations. More separated neighbors tend to have more oscillations in the frequency dependence.

The third is the out-of-phase motions of atoms in zone boundary longitudinal modes (33 meV). Overall, the preponderance of low frequency modes, especially at finite temperatures, favors the in-phase narrowing of the instantaneous RDF. As expected, one must consider all of the phonon modes in order to get a picture of the local atomic correlations. For the subsequent neighbors, the faster oscillation of the phase factor and weaker interatomic potential tends to reduce the effect (10% or less) and the inelastic structure contributes only weakly to the instantaneous RDF.

It is perhaps unexpected, for the nearest neighbor pair, that there are atomic correlations due to the phonon vibrations which are of sufficient amplitude to be measured. As is apparent from Fig. 4, the first RDF peak has a much narrower peak width as compared to more distant peaks. Thus, the effect of the thermal diffuse scattering on the instantaneous RDF of nickel should be observable in the diffraction experiment. In fact, it is observed in the instantaneous RDF measured by pulsed neutron scattering (at the Glass Liquid Amorphous Diffractometer at the Intense Pulsed Neutron Source of Argonne National Laboratory).[13] Figure 6, shows the experimental instantaneous RDF of nickel at 300 K plotted with the theoretical instantaneous RDF from Fig. 4. The first four experimental RDF peaks were fitted to the sum of four Gaussians using a least-squares fitting method. The inset

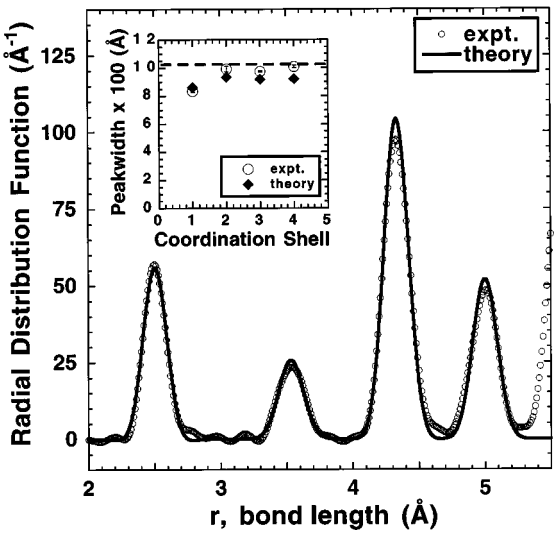

FIG. 6. Instantaneous RDF of nickel at $T=300$ K as measured with the Glass Liquid Amorphous Diffractometer at the Intense Pulsed Neutron Source of Argonne National Laboratory (Ref. 13). Plotted over the experimental data is the instantaneous RDF calculated from theory. The inset figure shows the fitted gaussian width of the experimental data and the theoretical widths for the first four coordination shells. The dashed line in the inset figure is the uncorrelated width (proportional to $\langle u^2\rangle^{1/2}$).

of Fig. 6 shows the theoretical and fitted experimental peak widths. The dashed line in the inset of Fig. 6 shows the peak width value which arises from entirely uncorrelated, single atom motion at $T=300$ K. Both the experimental and theoretical peak widths show the pronounced narrowing of the nearest neighbor peak as compared to the more distant peaks and the uncorrelated width. The more more distant coordination shells show a small degree of correlation. Thus, the effect of local atomic correlation can be observed from a diffraction experiment. This is perhaps not very surprising. The RDF is obtained from the diffraction data by Fourier transforming all of the intensity contained in $S(Q)$ including the diffuse scattering. The thermal diffuse scattering is highly structured in Q space, having power law tails near Bragg points due to the large occupancy of low frequency phonons. Consequently, it will contribute additional structure to the RDF above that from the Bragg scattering.

IV. CONCLUSION

Much of the strength of inelastic pulsed-neutron chopper spectrometers lies in the ability to measure the Q dependencies of $S(Q,\omega)$, at any frequency, up to very large momentum transfer. For amorphous or polycrystalline samples, this Q dependence is related to the spatial distribution and relative displacement directions for atoms vibrating at a given frequency. Thus, the inelastic portion of $S(Q,\omega)$ amounts to the energy-resolved diffuse scattering from the sample. This diffuse scattering can have many origins for many different materials, such as phonons, local modes, polarons, etc. In cases where such local atomic motions are of interest, the

Fourier transform of $S(Q,\omega)$ over the spatial coordinates gives a local, dynamic function $g(r,\omega)$.

The transform of $S(Q,\omega)$ to $g(r,\omega)$ is defined in an analogous manner to the radial distribution function (RDF) (or pair-distribution function) obtained from diffraction measurements. In this fashion, $g(r,\omega)$ is a probability conserving function in the sense that either the average (elastic) RDF or instantaneous (energy-integrated) RDF can be obtained. The main outcome of this statement is that the structure contributed to the instantaneous RDF from the inelastic scattering can only displace or change shape compared to the average RDF, while conserving the peak area. The prescription to follow is to obtain both the instantaneous and average RDF from $g(r,\omega)$, since differences in these RDFs implies the existence of local and dynamic atomic correlation. Using the ability of inelastic neutron scattering to resolve the energy transfer, one can then determine at which frequencies the local distortions are occurring.

To demonstrate these ideas, the dynamic radial distribution function $g(r,\omega)$ was calculated for atomic displacements due to phonons in fcc nickel. A difference in the instantaneous RDF and average RDF is observed for the nearest neighbor peak, where the instantaneous RDF peak is narrower than the average, implying that local correlation due to phonon vibrations tends to move the atomic pair in-phase. This observation is supported by instantaneous RDF measurements from neutron diffraction. By looking into the frequency dependence at constant r equal to the nearest neighbor pair distance, it is apparent that the in-phase correlation comes from the preponderance of low-frequency, long wavelength phonons. This can be understood by considering that the phonons in nickel produce thermal diffuse scattering, which is observed as tails of the Bragg peak in reciprocal space. The thermal diffuse scattering is therefore highly structured in reciprocal space and contributes additional local structure to the instantaneous RDF.

The calculations on nickel, and their comparison to diffraction data, demonstrate two important conclusions. First, the RDF analysis of diffraction data represents the instantaneous structure of the material and the observed atomic correlations originate from the thermal diffuse scattering. Second, the extraction of the local dynamic structure function allows one to determine which atomic pairs have correlated motion by comparison of the instantaneous and average RDF and consequently to determine the frequencies. The energy-resolved $g(r,\omega)$ measurements are therefore unique probes which bridge the gap between slow and fast local probes in a consistent manner.

ACKNOWLEDGMENTS

The author is grateful to R. A. Robinson, T. Egami, D. Louca, and W. Dmowski for extremely helpful discussions and assistance with experimental data. This work is supported in part by the division of Basic Energy Sciences of the U.S. Department of Energy.

APPENDIX

The dynamic pair correlation function is defined by Eq. (1) with the weighting function $f(Q)=1/Q^2$. While the frequency-dependent correlation functions of the DPCF are identical to those of the dynamic distribution function $g(r,\omega)$, the radial functions differ due to $f(Q)$. The DPCF inelastic radial functions, denoted $K_2'(r)$ and $K_0'(r)+K_2'(r)$, are shown in Fig. 7. The benefit of the weighting factor is that the inelastic structure function $K_2'(r)$ has a single peak at the atomic pair distance, similar to a RDF peak. Thus, this formulation is quite useful for direct comparison of the DPCF at a particular frequency to the RDF. It is also possible that dynamic features will be more prominent in some cases, due to the single peak. However, the DPCF radial functions have tails extending below the peak. This becomes a more severe problem for short and intermediate pair distances, since the inelastic structure contains contributions of all pairs longer than the given pair distance. Consequently, one cannot speak of a probabilistic interpretation of the DPCF and cannot calculate the true RDFs.

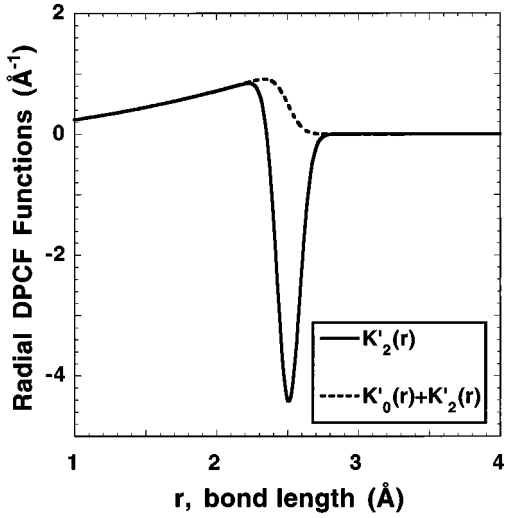

FIG. 7. The dynamic pair correlation function (DPCF) inelastic radial functions, $K_2'(r)$ and $K_0'(r)+K_2'(r)$. $K_2'(r)$ has a single peak at the pair distance, unlike the dynamic RDF radial function, $K_2(r)$, which has a W shape. Consequently, the DPCF formalism is more useful for identifying inelastic features, However, the DPCF peak has a long tail on the low-r side, making it difficult to determine the strength of atomic correlation.

As we have seen, the Fourier transform of $j_0(x)$ is a δ function (convoluted with a Gaussian Debye-Waller factor). The Fourier transform of $j_2(x)$ consists of a δ function plus a step function giving the characteristic DPCF functions. Retaining the factor of Q^2 in our formulation is equivalent to taking twice the derivative of the DPCF with respect to r (exactly, $-d^2/dr^2$). This operation removes the step and relegates the inelastic intensity to within $\sim\langle u^2\rangle^{1/2}$ of the pair position. The penalty for this operation is that the $K_2(r)$ radial functions no longer contain a single peak, but have a W shape. As has been shown, this is precisely the functional form required to preserve the overall probability between the average and instantaneous RDFs. Thus, the dynamic RDF and DPCF formulations both have benefit in the analysis of the dynamic features in the inelastic experiment.

[1] T. Egami and S. J. L. Billinge, Prog. Mater. Sci. **38**, 359 (1994).
[2] T. Egami and S. Billinge, in *Physical Properties of High Temperature Superconductors V*, edited by D. Ginsberg (World Scientific, Singapore, 1996).
[3] S. J. L. Billinge *et al.*, Phys. Rev. Lett. **77**, 715 (1996).
[4] J. M. Carpenter and C. A. Pelizzari, Phys. Rev. B **12**, 2391 (1975).
[5] J. M. Carpenter and C. A. Pelizzari, Phys. Rev. B **12**, 2397 (1975).
[6] A. C. Hannon, M. Arai, and R. G. Delaplane, Nucl. Instrum. Methods Phys. Res. A **354**, 96 (1995).
[7] A. C. Hannon *et al.*, J. Non-Cryst. Solids **150**, 239 (1992).
[8] M. Arai *et al.*, Physica B **180&181**, 779 (1992).
[9] M. Arai *et al.*, J. Non-Cryst. Solids **192&193**, 230 (1995).
[10] M. Arai *et al.*, J. Supercond. **7**, 415 (1994).
[11] T. Egami, Mater. Trans., JIM **31**, 163 (1990).
[12] T. Egami (unpublished).
[13] D. Louca (unpublished).
[14] R. J. McQueeney, Ph.D. thesis, Dept. of Physics, University of Pennsylvania, Philadelphia, 1996.
[15] S. W. Lovesey, *Theory of Neutron Scattering From Condensed Matter* (Oxford University Press, New York, 1984).
[16] J. M. Carpenter, J. Chem. Phys. **46**, 465 (1967).
[17] B. E. Warren, *X-ray Diffraction* (Dover, Mineola, NY, 1990).
[18] R. J. Birgenau *et al.*, Phys. Rev. **136**, A1359 (1964).